doi:10.14311/ppt.2017.1.56
Plasma Physics and Technology **4**(1):56–59, 2017
© Department of Physics, FEE CTU in Prague, 2017

ANALYSIS OF RADIATION DISCRETIZATION FOR MODELLING A SPARK GAP FOR SURGE CURRENTS

C. Sander[a,b,*], J.-E. Schmutz[a], M. Kurrat[b]

[a] *PHOENIX CONTACT GmbH & Co. KG, Flachsmarktstraße 8, D-32825 Blomberg, Germany*

[b] *Institute for High Voltage Technology and Electrical Power Systems, Technical University Braunschweig, Schleinitzstraße 23, 38106 Braunschweig, Germany*

[*] christian.sander1@phoenixcontact.com

Abstract. In this paper we address a method for spectrally resolved radiation modelling in thermal plasmas encountered in surge protective devices based on spark gaps. Compared to most switching applications, power input and plasma pressure are much higher which leads to an optically thick plasma with line broadening and enhanced wall ablation. In this situation it is possible to capture the full effect of spectrally resolved radiation on plasma dynamics by performing line-by-line calculations with downsampled absorption spectra. We show that it is possible to achieve radiation convergence with 1000 lines. Approaches for a further reduction of calculation times using band-averaged models and κ-group models are discussed. The κ-group model is based upon a grouping of the absorption coefficients into subgroups with different ranges of κ before averaging. The spectral calculation results are compared to the approximative methods and significant differences for Rosseland means are observed.

Keywords: spark gap, radiation, spectral, simulation, arc, surge protective device.

1. Introduction

Simulation of surge protective devices (SPDs) [1] has received considerably less attention than other devices employing thermal plasmas such as circuit breakers. Nontheless, the challenges faced here are similar, if not more difficult, due to the higher power density leading to a wider range of temperatures, pressures, and dynamics. Spark-Gap SPDs make use of wall stabilized arcs with small channel diameters which are needed for arc extinction and net follow current suppression. These kinds of arcs are influenced by interaction with the enclosing walls. Ablation occurs mainly because of radiation, so a large emphasis needs to be put on precise modelling of radiative transport. This is a considerable challenge because of the complex spectral dependence of absorption coefficients. Peyrou et al. investigated the precision of methods for solving the radiative transfer equation and the effects of spectral averaging methods[2]. They found reasonably good results using the Rosseland average for a multi-band model of 11 bands in optically thick conditions. Nordborg et al. used a subdivision of the bands according to the value of the absorption coefficient to reduce averaging errors with good results [3]. Randrianandraina et al. use a combination of Planck and natural averages based on frequency of the band and on temperature to obtain better results with a multi-band model[4].

In this paper we'll present time-dependent simulations of an SPD using a downsampled line-by-line method and compare it with band-averaged methods and the κ-group model used by Nordborg et al.[3].

2. Simulation model

The simulation is based on the assumption of local thermodynamic equilibrium and electrical quasi-neutrality. These assumptions result in the classical Navier-Stokes equations with additional terms for ohmic heating, radiation, electron enthalpy transport and ablation. Magnetic forces are smaller than pressure forces for the conditions discussed here and are neglected for better performance (less than 1 % difference).

$$\frac{\partial \rho}{\partial t} + \vec{\nabla}\cdot(\rho\vec{U}) = S_\rho \tag{1}$$

$$\frac{\partial \rho\vec{U}}{\partial t} + \vec{\nabla}\cdot(\rho\vec{U}\otimes\vec{U}) = \vec{\nabla}\cdot\boldsymbol{\tau} - \vec{\nabla}p \tag{2}$$

$$\frac{\partial \rho(h+k+\frac{p}{\rho})}{\partial t} + \vec{\nabla}\cdot(\rho(h+k)\vec{U}) = S_e + h_{S_\rho}S_\rho \tag{3}$$

In these equations ρ denotes density, $\vec{U}$ velocity, S_ρ the mass source term (see eq. 9), $\boldsymbol{\tau}$ the viscous stress tensor, p pressure, h enthalpy, k kinetic energy and h_{S_ρ} the enthalpy of the ablated mass entering the fluid region. The term S_e contains all sources that increase the internal energy and the kinetic energy:

$$S_e = \frac{\vec{j}^2}{\sigma} + S_R - \vec{\nabla}\cdot(\lambda\vec{\nabla}T) + \frac{5k_B}{2q_e}\vec{j}\cdot\vec{\nabla}T + \vec{\nabla}\cdot(\boldsymbol{\tau}\cdot\vec{U}) \tag{4}$$

Here $\frac{\vec{j}^2}{\sigma}$ is the ohmic heating, S_R the radiative source term, $\vec{\nabla}\cdot(-\lambda\vec{\nabla}T)$ the heat conduction source term, $\frac{5k_B}{2q_e}\vec{j}\cdot\vec{\nabla}T$ the enthalpy transport by electrons with k_B being the Boltzmann constant and q_e the elementary charge and $\vec{\nabla}\cdot(\boldsymbol{\tau}\cdot\vec{U})$ the viscous heat. The

electrostatic potential ϕ is calculated as

$$\vec{\nabla}\cdot(\sigma\vec{\nabla}\phi) = 0 \tag{5}$$

which gives the electric current as $\vec{j} = -\sigma\vec{\nabla}\phi$, with σ being the electrical conductivity.

Radiation is considered in the P1-model, which gives the following equations in its spectral form [5]:

$$\vec{\nabla}(\frac{1}{3\kappa_\nu}\vec{\nabla}G_\nu) = \kappa_\nu(G_\nu - 4\pi B_\nu(T)) \tag{6}$$

$$S_R = \vec{\nabla}\cdot(\int \frac{1}{3\kappa_\nu}\vec{\nabla}G_\nu \,\mathrm{d}\nu) \tag{7}$$

To consider the effect of plasma-wall interaction, we model the ablation of the polyoxymethylene (POM) wall by solving a heat balance equation (eq. 8) at the surface, considering heat conduction from plasma into the solid, radiation and the ablation heat flux of the ablated material going into the plasma. Ablation starts once the surface temperature reaches the evaporation temperature of POM which is taken as $T_v = 683\,\mathrm{K}$. We assume that the wall temperature cannot exceed the evaporation temperature, which allows to determine the required ablative heat flux needed for limiting the temperature.

$$q_{c,p} + q_r = q_{c,f} + q_v \tag{8}$$

$$S_\rho = \frac{q_v A}{\Delta h_{v,\mathrm{eff}} V} \tag{9}$$

Here A is the surface area of a boundary cell and V its volume. $\Delta h_{v,\mathrm{eff}} = \Delta h_v + (h(p, T_k) - h(p_0, T_v))$ is the enthalpy change of the gas which is ablated. It is commonly accepted that ablated gas enters the plasma at a much higher temperature than T_v because radiation is absorbed in the intermediate layer close to the wall [6]. We assume a temperature of the ablated gas of $T_k = 3500\,\mathrm{K}$ and an evaporation enthalpy of $\Delta h_v = 1.6\,\mathrm{MJ/kg}$. For electrode erosion we consider a simple model in which the mass source term is proportional to current density [7].

The plasma composition, thermodynamic and transport properties of the plasma are taken from D'Angola et al. [8], hence we assume that the plasma consists of air only. The radiative absorption coefficient $\kappa_\nu(p, T)$ is calculated with SPARTAN [9], which is freely available.

The simulation model was implemented in OpenFOAM [10] using the flow solver published by Kraposhin et al.[11].

In spark gaps an ignition circuit is often used to facilitate plasma ignition at lower voltages than the very high breakdown voltage of the main electrodes (see figure 1). A third electrode is connected by a metal-oxide varistor to the first main electrode and placed near the second main electrode. Ignition then happens by electric breakdown or resistive elements at much lower voltage. The nonlinearity of the varistor characteristic curve is solved by employing the linearity of equation 5, separating it into multiple equations

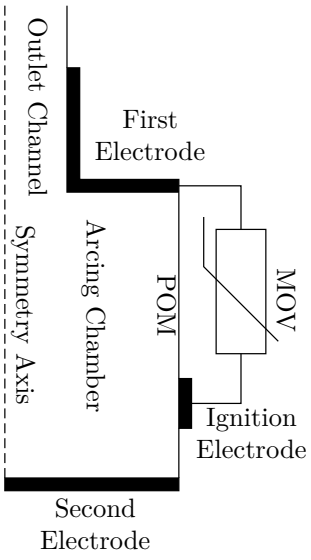

Figure 1. Investigated geometry with ignition circuit.

where only one of the electrodes has a potential $\phi_i \neq 0$ and then using superposition to calculate the full potential. This allows to reduce the iterative procedure of finding the correct potentials to a problem that doesn't require the repeated solving of equation 5.

The simulation is started at ambient conditions. To make the ignition possible, an artificially increased conductivity value is assumed in the area between the ignition electrode and the second electrode for a short amount of time. An $8/20\,\mu\mathrm{s}$ waveform impulse with an amplitude of $15\,\mathrm{kA}$ is impressed between the main electrodes. No-slip boundary conditions are used and on the outer side of the solids we apply spatially constant potentials and ambient temperature. The calculations shown here were performed on an Intel i7-4770 using one thread.

3. Averaging methods

We employ the following methods for handling the spectral dependence of radiation:

1. Spectrally resolved absorption coefficients $\kappa_\nu(p, T)$, possibly downsampled for better performance

2. Mean absorption coefficients (MACs) band model for spectrally separated bands $\kappa_i(p, T)$, namely Planck, Rosseland and Natural means

3. κ-group model, based on subdividing each band from 2. into discontinous groups depending on the value of $\kappa_\nu(p, T)$ and averaging these groups resulting in a set of absorption coefficients $\kappa_{i,j}(p, T)$

Spectrally resolved absorption coefficients can return exact results at the price of very high computational cost. Because of this we employ a coarse mesh to be able to handle spectral discretizations of up to 10^5 points. Calculation of MACs are performed using the frequency intervals $[3 \cdot 10^{-5}, 0.35, 1.54, 2.65, 2.94, 3.51, 15] \cdot 10^{15}\,\mathrm{s}^{-1}$ ([7] extended for broader spectral

N_ν	U	$\overline{T}$	T_{max}	$\overline{p}$	m	t
	V	K	K	bar	kg	h
10^5	403.6	28884	44905	936.1	4.22e-9	280
	ΔU	$\Delta\overline{T}$	ΔT_{max}	$\Delta\overline{p}$	Δm	t
	%	%	%	%	%	%
10^4	0.06	-0.03	-0.07	-0.07	0.10	13
5000	0.04	-0.03	-0.15	-0.13	-0.02	6.5
1000	0.35	-0.20	-0.19	0.02	0.78	1.4
100	n. c.	n. c.	n. c.	n. c.	n. c.	n. c.

Table 1. Absolute values of the most accurate calculation with $N_\nu = 10^5$ frequency sampling points and relative errors with fewer sampling points at $t = 10\,\mu s$

range) and $[0.075, 0.350, 1.540, 2.114, 2.180, 2.430, 2.563, 2.900, 3.260, 3.350, 3.520, 3.750, 4.200, 5.960, 6.561, 7.048, 7.840, 11.00, 15.00] \cdot 10^{15}\,\mathrm{s}^{-1}$ (based on $\kappa_\nu(p,T)$ dependency). A method of choosing the subgroups based on the value of κ_ν is required for the κ-group model. Because SPARTAN outputs an irregular frequency axis it was necessary to resample the spectra to a regular axis with $2 \cdot 10^7$ points. Because of the pressure and temperature dependence it is not possible to sort a specific κ_ν value uniquely into one group for all pressures and temperatures. Instead of using global definitions for the boundaries of the groups we define them separately for each pressure and temperature based on the minimum and maximum values of κ_ν encountered in one band. The groups are equidistantly spaced on the logarithmic scale. This method results in a different mapping of κ_ν for each pressure and temperature. We can calculate a mean group for every frequency point and use this as a mapping for all absorption spectra. In the end one of the different absorption means is calculated for the set of frequencies contained in each band/group tuplet resulting in a set of $\kappa_{i,j}(p,T)$ values. If one of these sets is empty it will be dropped.

4. Results

The convergence behaviour of the spectrally resolved calculations is shown in table 1 along with calculation times. The values are evaluated at current maximum ($t = 10\,\mu s$) when a wall stabilized arc is formed. At $N_\nu = 100$ the simulations didn't converge, however for discretizations with $N_\nu \geq 1000$ the error is less than 1 % for all quantities, showing a good convergence for a much lower sampling rate than the complexity of the spectrums suggests. We attribute this to the relatively high optical thickness occuring at large pressures at magnitudes above 100 bar, leading to line broadening which thus requires less points. Moreover the mesh size is larger than the optical thickness for many frequencies which may also have an influence. During the ignition ($t < 4\,\mu s$) there are some deviations in the maximum encountered temperature between 100000 and fewer points (not listed in the table) but

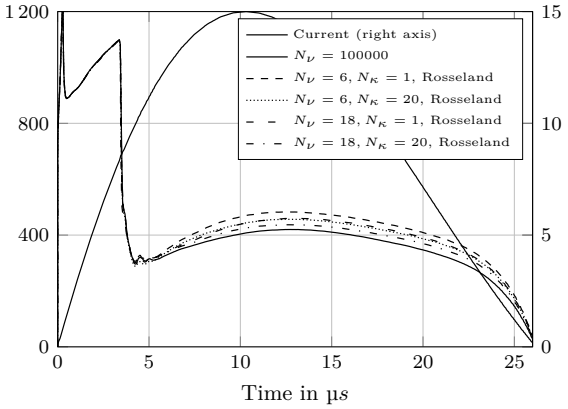

Figure 2. Current impulse and voltages of band models and κ-grouped models compared to the most accurate spectrally resolved calculation. (Left axis: Voltage in V, right axis: Current in kA)

this doesn't have a significant influence on the further behaviour. We take the calculation with 100000 sampling points as reference for all further calculations because the difference seen in comparison with fewer sampling points suggests the correctness of this result. Higher discretizations were not performed because of calculation times.

Figure 2 shows exemplary voltage curves of Rosseland-averaged band and κ-group models for the two spectral intervals discussed before. The Rosseland average is displayed because it represents the worst case of the Planck, Natural and Rosseland means. It can be seen that the voltage during the ignition phase and the ignition time are mostly unaffected by the means of radiation approximation. This is largely caused by the low amount of ablation that happens in this phase. Differences start to appear after the ignition when ablation becomes relevant. Increasing the spectral bands and/or number of κ-groups leads to better results in all cases but also increases calculation times (Approximately doubled calculation time for $N_\nu = 6, N_\kappa = 20$ compared to $N_\nu = 6, N_\kappa = 1$).

The average temperature of κ-group models with $N_\nu = 18, N_\kappa = 20$ and different averaging methods is shown in figure 3. All methods show little deviations compared to the exact result, however the Rosseland mean underpredicts the mean temperature the most.

Table 2 shows the percental errors of voltage, average temperature, maximum temperature, average pressure and total ablated mass in the arcing chamber at $t = 10\,\mu s$ and the percentage of calculation time compared to the spectrally resolved calculation with 100000 sampling points. The choice of Rosseland average results in the largest errors of voltage and ablation mass. At the same time the Rosseland average gives a very good fitting to the maximum temperature.

The Rosseland average overpredicts the emission in the arc core, leading to a stronger ablation and a stronger cooling in the boundary regions, thus the arc is more constricted and a larger current density and

N_ν	N_κ	$\overline{\kappa}$	ΔU	$\Delta \overline{T}$	ΔT_{max}	$\Delta \overline{p}$	Δm	Δt
6	1	P	4.98	-0.76	7.05	-8.23	-2.52	0.14
6	1	N	0.89	1.90	5.56	-1.76	1.30	0.12
6	1	R	15.2	-6.98	-0.08	5.97	32.0	0.13
6	20	P	4.17	-0.35	6.76	-3.36	3.00	0.26
6	20	N	2.08	0.03	5.27	-1.66	2.49	0.25
6	20	R	8.86	-4.07	1.49	5.28	21.6	0.27
18	1	P	5.91	-0.49	3.14	-6.35	2.32	0.14
18	1	N	3.03	0.53	6.46	-3.36	1.53	0.14
18	1	R	8.67	-4.10	0.55	1.36	15.9	0.14
18	20	P	4.76	-0.94	4.07	-2.08	5.07	0.48
18	20	N	3.95	-0.49	4.12	-1.50	4.85	0.47
18	20	R	4.41	-1.99	0.25	-0.63	6.03	0.49

Table 2. Relative errors and calculation time (in %) of radiation approximations at $t = 10\,\mu s$.

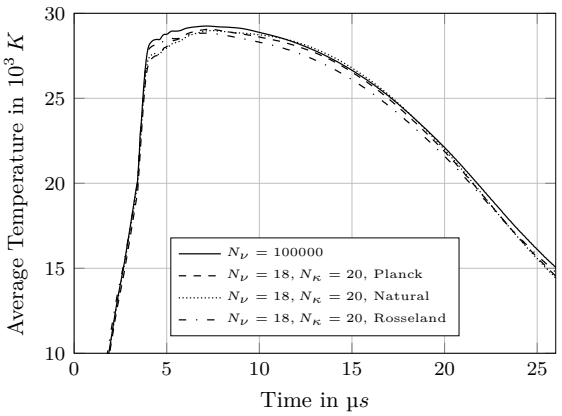

Figure 3. Average temperature of reference calculation compared to different κ-group models radiation approximation methods.

ohmic heating is observed in the core which compensates the stronger emission. The enhanced ablation is also responsible for the lower average temperatures.

The Planck and Natural means both give very good results, with the natural mean being slightly better at most quantities. Using more bands doesn't lead to significantly better results. The reason is most likely an unoptimized choice in band limits and too much variation of the absorption coefficient in the single bands even when more bands are used. Using more κ-groups shows consistent improvements only for the Rosseland mean.

These results suggest to perform further optimizations or to use an averaging method that gives acceptable results at the lowest computation time. In this case we would favor the 6-band natural mean. Further optimization may improve the choice of band limits, employ line limiting methods or switch the averaging method in some ranges of pressures and temperatures.

5. Conclusions

We have investigated the accuracy of various methods of spectral discretizations. The use of downsampled absorption coefficients gave good results, making this a feasible method if the increased calculation time is acceptable. The well known band model gives good results compared to the spectrally resolved result when the Planck or natural means are used. The 6-band natural mean gives errors on the order of approximately 5 % and is more than 10 times faster than the fastest spectrally resolved calculation. However, the Rosseland mean results in a larger error and it cannot be recommended without further improvements. The grouping of the absorption coefficient based on its value gives improved results, however there is still a difference to be observed. It is possible that the accuracy of these approximations can be improved by line limiting or by the selective use of different MACs. It might also be possible to get better results by an optimized choice of band and group limits.

References

[1] Phoenix Contact GmbH & Co. KG. Lightning and surge protection basics. `https://www.phoenixcontact.com/assets/downloads_ed/global/web_dwl_promotion/5131327_TT_Basics_EN.pdf`, 2017.

[2] B. Peyrou et al. Radiative properties and radiative transfer in high pressure thermal air plasmas. *J. Phys. D: Appl. Phys.*, 45(45):455203, 2012. `doi:10.1088/0022-3727/45/45/455203`.

[3] H. Nordborg and A. A. Iordanidis. Self-consistent radiation based modelling of electric arcs: I. efficient radiation approximations. *J. Phys. D: Appl. Phys.*, 41(13):135205, 2008. `doi:10.1088/0022-3727/41/13/135205`.

[4] H. Z. Randrianandraina et al. Improvements of radiative transfer calculation for SF_6 thermal plasmas. *J. Phys. D: Appl. Phys.*, 44(19):194012, 2011. `doi:10.1088/0022-3727/44/19/194012`.

[5] Michael F. Modest. *Radiative Heat Transfer, Third Edition.* Academic Press, 3 edition edition.

[6] D. Godin et al. Modelling and simulation of nozzle ablation in high-voltage circuit-breakers. *J. Phys. D: Appl. Phys.*, 33(20):2583, 2000. `doi:10.1088/0022-3727/33/20/310`.

[7] C. Rümpler. *Lichtbogensimulation für Niederspannungsschaltgeräte.* Fraunhofer-Verlag, 2009.

[8] A. D'Angola and other. Thermodynamic and transport properties in equilibrium air plasmas in a wide pressure and temperature range. *Eur. Phys. J. D*, 46(1):129–150, 2008. `doi:10.1140/epjd/e2007-00305-4`.

[9] Lino da Silva, M. An adaptive line-by-line—statistical model for fast and accurate spectral simulations in low-pressure plasmas. *J. Quant. Spectrosc. Radiat. Transfer*, 108(1):106–125, 2007. `doi:10.1016/j.jqsrt.2007.03.005`.

[10] H. Jasak. OpenFOAM: Open source CFD in research and industry. *Int. J. Nav. Archit. Ocean Eng.*, 1(2):89–94, 2009. `doi:10.2478/IJNAOE-2013-0011`.

[11] M. Kraposhin et al. Adaptation of kurganov-tadmor numerical scheme for applying in combination with the PISO method in numerical simulation of flows in a wide range of mach numbers. *Procedia Comput. Sci.*, 66:43–52, 2015. `doi:10.1016/j.procs.2015.11.007`.